Conformational Differences Between O- and C-Glycosides: The α-*O*-Man-(1 $\rightarrow$1)-β-Gal/α-*C*-Man-(1 $\rightarrow$1)-β-Gal Case— A Decisive Demonstration of the Importance of the *exo*-Anomeric Effect on the Conformation of Glycosides

Juan L. Asensio,[a] F. Javier Cañada,[a] Xuhong Cheng,[b] Noshena Khan,[b] David R. Mootoo,*[b] and Jesús Jiménez-Barbero*[a]

Dedicated to Prof. Dr. Martín-Lomas on the occasion of the new millenium

Abstract: The conformational behavior of α-O-Man-(1 $\rightarrow$1)-β-Gal (**1**) and its C-analogue (**2**) has been studied using *J*/NOE NMR data, molecular mechanics, molecular dynamics, and ab initio calculations. The population distribution around the glycosidic linkages of **1** and **2** is rather different, especially for the α-Man linkage. A lower limit for the *exo*-anomeric effect in water has been experimentally determined.

Keywords: C-glycosides · conformation analysis · molecular modeling · NMR spectroscopy · selectin

Introduction

Carbohydrate–protein interactions are involved in a wide range of biological activities starting from fertilization and extending to pathological processes such as tumor growth.[1, 2] Since the carbohydrate ligands are object to hydrolytic degradation, C-glycosides have been developed to improve chemical and biochemical stability.[3, 4] Thus C-glycosides[3] have attracted interest as hydrolytically stable analogues of O-saccharides and are being applied as enzyme inhibitors and/or to mimic carbohydrate–protein interactions. However, the conformational similarity of the intersaccharide linkage has been under debate since stereoelectronic effects due to the presence of the interglycosidic oxygen would be absent in the C-glycoside,[6b] and steric interactions between both residues are expected to be different (due to disimilar C–O versus C–C bond distances and C-O-C versus C-C-C angles). Indeed, appreciable differences between O- and C-glycosides with respect to conformational behavior and activity have been reported.[4, 5] It has been suggested that C- and O-glycosides as exemplified by C-/O-lactose share the same conformational characteristics in the free state.[7] The findings that the bound conformation of C-lactose to peanut agglutinin is identical to that of its parent O-lactose bound to this lectin was quoted by these authors as additional evidence of the conformational similarity between O-/C-glycosides.[7] However, we recently noted that this assumption is invalid at least for C-/O-lactose (β-(1 $\rightarrow$4)-linkage)[5a–c] and for C-/O-mannobiose (α-(1 $\rightarrow$2)).[5d] Our studies indicate that the conformational behavior of each C-/O-pair is similar about the glyconic bond but significantly different about the aglyconic bond. In order to further probe the enhanced flexibility around the glyconic linkages of C-glycosides, we have extended these studies to α-*O*-Man-(1 $\rightarrow$1)-β-Gal (**1**) and its C-analogue **2**. The result of this investigation is reported herein.

Our initial interest in **1** and **2** stems from the hypothesis that **1** is a mimic of the Gal-GlcNAc-Fuc part of sLeX.[8] Indeed, substitution of Gal-*O*-3 of **1** with a carboxymethyl group leads

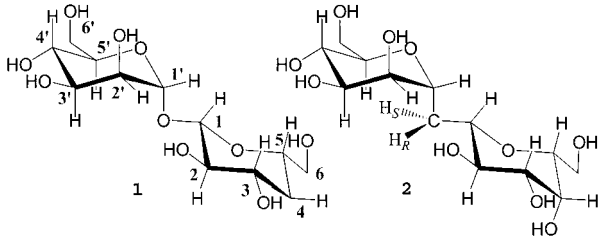

to a compound which is five times as active as sLeX in binding to E-selectin.[8] Thus, its corresponding C-glycosyl analogue **2** could be a potential therapeutic agent. Compounds **1** and **2**

[a] Dr. J. Jiménez-Barbero, Dr. J. L. Asensio, Dr. F. J. Cañada
Departamento de Química Orgánica Biológica
Instituto de Química Orgánica, CSIC
Juan de la Cierva 3, 28006 Madrid (Spain)
E-mail: IQOJ101@fresno.csic.es

[b] Dr. D. R. Mootoo, Dr. X. Cheng, N. Khan
Department of Chemistry
Hunter College City University of New York, NY (USA)

  0947-6539/00/0606-1035 $ 17.50+.50/0

are of additional interest for several reasons. It is known that besides stereoelectronic effects, steric interactions may also play an important role in determining the conformational behavior of natural oligosaccharides. In absence of the *exo*-anomeric effect, the conformational properties of C-glycosides should be heavily influenced by 1,3-type diaxial steric interactions. Thus, the non-*exo*-anomeric (Figure 1) orientation around α- or β-Glc or Gal bonds is expected to be destabilized by a 1,3-type diaxial interaction between the equatorial OH2 and the aglycon. In contrast, for α- or β-Man configuration the non-*exo* orientation does not present 1,3-type interaction between the substituent at position 2 and the aglycon. According to this hypothesis, the Man-configuration on one side of the linkage for **1** and **2** was chosen to make the *exo-syn* (Scheme 1) and the non-*exo* orientation from the steric point of view equally accessible. At the same time, the *manno* form may allow the unequivocal detection of non-*exo* conformers through measurements of exclusive NOEs (see below). In addition, compounds **1** and **2** were chosen because both intersaccharide bonds are glyconic: **1** shows overlapping *exo*-anomeric effects. Thus at any linkage, the stereoelectronic effect is expected to be smaller than that for regular saccharides. Comparison of **1** (O-glycoside with attenuated *exo*-anomeric effect) versus **2** conformer distributions could shed light on the magnitude of the stereoelectronic effect and clarify the controversy on O/C-glycoside conformational similarity.[5, 7]

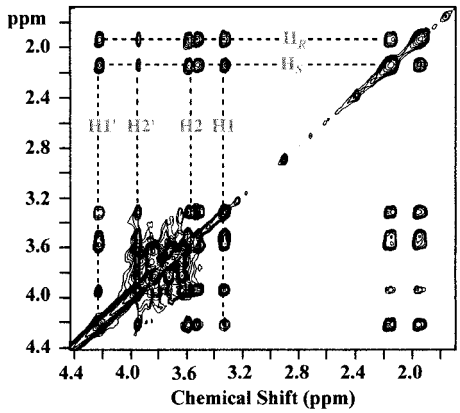

Figure 1. 2D-TOCSY (mixing time 100 ms) spectrum of **2** (500 MHz, 310 K, D_2O). Key ^{1}H-NMR assignments are shown. 3-(Trimethylsilyl)-1-propane-sulfonic acid (DSS) was used as internal reference.

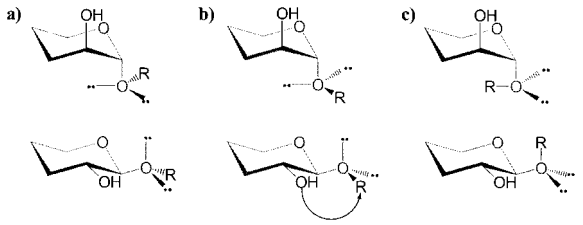

Scheme 1. Schematic representation of the a) *exo-syn* b) non-*exo* and c) *exo-anti* orientation for the aglycon R in a α-mannoside and a β-galactoside.

Abstract in Spanish: *El comportamiento conformacional del α-O-Man-(1 $\rightarrow$1)-β-Gal (**1**) y su análogo C-glicosídico **2** se ha estudiado utilizando una combinación de datos experimentales de RMN y cálculos de mecánica y dinámica molecular y ab initio. La distribución de poblaciones en torno a los enlaces glicosídicos de **1** y **2** es muy distinta, especialmente para el enlace α-Man. Además, se ha determinado experimentalmente un límite inferior para el efecto exo-anomérico en disolución acuosa.*

Results and Discussion

The ^{1}H-NMR spectra of compounds **1** and **2** were assigned by standard methods using a combination of TOCSY, DQF-COSY, NOESY and HMQC. The intra-ring vicinal proton–proton coupling constants (data not shown) proved that all six-membered rings adopt the $^4C_1$(D) conformation, independent of the stereochemistry at *C*-2. Diastereotopic assignment of the prochiral H_R and H_S protons was performed using a similar protocol to that described previously[5d] based exclusively on a combination of *J* and NOE values.

Molecular mechanics calculations: As a first step to deduce the conformational behavior of compounds **1** and **2**, their potential energy surfaces were calculated using the MM3* force field, as described[5d] and are shown in Figure 2. These surfaces provide a first estimation of the conformational regions which are energetically accessible. Two main conformational families are found for **1** (Figure 2). The global minimum A (*exo-syn*/*exo-syn*) is populated about 99%. This conformation is in agreement with the presence of the *exo*-anomeric effect around both linkages.[6] Local minima B (non-*exo*/*exo-syn*) and C (*exo-syn*/*exo-anti*) are barely predicted. The low-energy region that corresponds to minimum A is extended towards negative Φ_{Gal} values (*exo-syn*/non-*exo* region), although there is not any local minimum in this part of the potential energy map. In contrast, for compound **2**, the MM3* potential energy surface predicts the existence of five conformational families: A (66.8% *exo-syn*/*exo-syn*), B

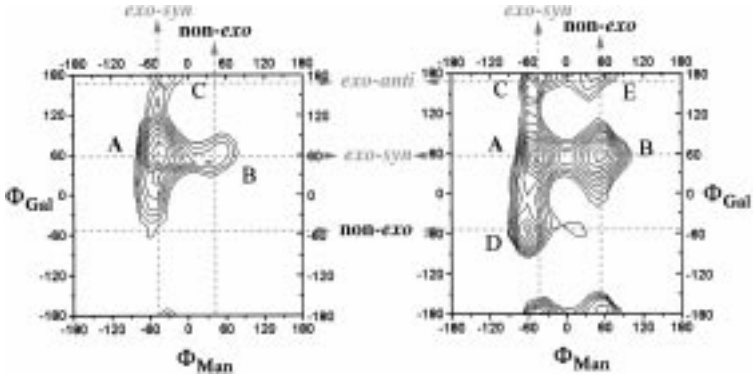

Figure 2. Steric energy maps calculated by the MM3* program with $\varepsilon = 80$. Left for **1** and right for **2**. Contours are given every 2 kJ mol^{-1}. The main regions are marked.

0947-6539/00/0606-1036 $ 17.50+.50/0 *Chem. Eur. J.* **2000**, *6*, No. 6

(20.4% non-*exo*/*exo-syn*), and D (8.4% *exo-syn*/non-*exo*) are the major families (Figure 2). Minima C (3.3% *exo-syn*/*exo-anti*) and E (1.1% non-*exo*/*exo-anti*) are minor. A qualitative conformational analysis was reported for the 3-*O*-carboxy derivative of **1**.[8] Our conformational analysis of **1** and **2** is based on exclusive[9] interresidue NOEs[10] and *J* coupling data that characterize minima A-E (Figure 3). For **1** and **2**, the relevant NOEs are H1′-H1 (A), H1′-H2 (C), H2′-H1 (B) and H2′-H2 (E). Since the NOE intensities are sensitive to the respective conformer populations, a first indication of the population distribution could be obtained by focusing on these key NOEs. Significant differences between **1** and **2** can be observed (Figure 4). For **1** the strong H1′-H1 NOE shows, at least qualitatively, that the global minimum A (*exo-syn*/*exo-syn*) is highly populated in water. The additional small NOEs indicate a very minor presence of conformers B and C. By contrast, compound **2** shows medium–large H1′-H1 and H2′-H1, and medium H1′-H2 NOEs with different mixing times. Qualitatively, this observation is in agreement with an enhanced flexibility of **2** in comparison to **1**. In addition, it unequivocally shows the existence of a significant population around minimum B (characterized by a non-*exo*-anomeric orientation of the α-Man linkage) in agreement with the MM3* predictions. The experimental NOEs were compared with the values obtained from the MM3* maps using a relaxation matrix approach[10] as described.[5] In addition, for compound **2**, interglycosidic proton–proton *J* values were derived from the potential energy surface. A fair fit was obtained for the NOE values of **1**. For compound **2** the four interglycosidic *J* values (observed [Hz]: $J(H1',H_R) = 7.1$, $J(H1',H_S) = 7.4$, $J(H1,H_R) = 3.1$, $J(H1,H_S) = 8.0$ Hz) were not fitted by the MM3* map (expected [Hz]: $J(H1',H_R) = 4.3$, $J(H1',H_S) = 8.6$, $J(H1,H_R) = 3.1$, $J(H1,H_S) = 9.7$).

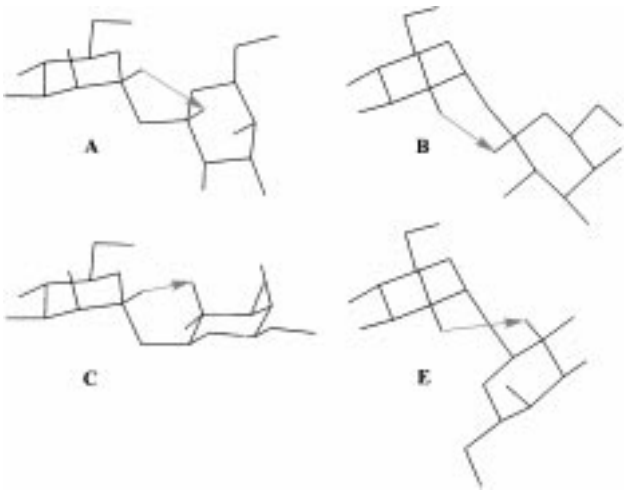

Figure 3. Simplified view of the major low-energy conformations obtained by MM3* calculations for compounds **1** and **2**. **A** (*exo-syn*/*exo-syn*), **B** (non-*exo*/*exo-syn*), **C** (*exo-syn*/*exo-anti*), **E** (non-*exo*/*exo-anti*). Expected exclusive and key NOEs are indicated for each conformer. For the α-Φ_{Man} torsion (H1′-C1′-X-C1), the *exo*-anomeric *syn* conformation is defined as $-60°$, the non *exo*-anomeric $+60°$, and the *exo-anti* 180°. For the β-Φ_{Gal} one (H1-C1-X-C1′), the *exo*-anomeric *syn* conformation is defined as $+60°$, the non-*exo*-anomeric $-60°$ and the *exo-anti* 180°.

Therefore, although no quantitative agreement between the MM3* predictions and the experimental NMR data for **2** was obtained, both sets of data indicate a rather different conformational behavior of the O-disaccharide in comparison with its C-analogue. The conformational space available to **2** is much larger than the corresponding one for **1**. For the former, there are also significant populations of conformers characterized by non-*exo*-anomeric orientations, especially for the ϕ_{Man} linkage.

ab initio Calculations: It is important to bear in mind that the MM3* force field is not parametrized to deal with systems presenting overlapping *exo*-anomeric effects, such as **1**. Thus, in order to gain insight into the consequences of this feature,

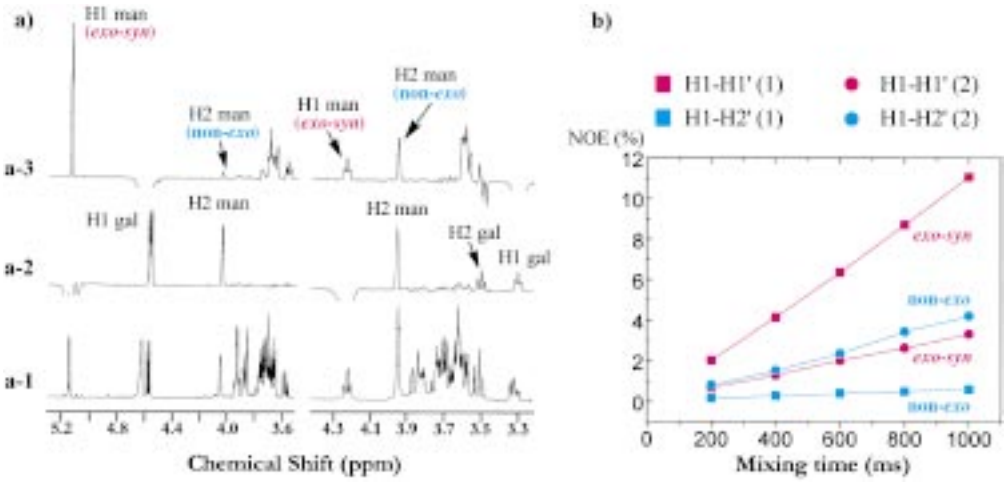

Figure 4. a) 1D-DPFGSE NOESY spectra of **1** (left) and **2** (right). (500 MHz, 310 K, D_2O, mixing time 800 ms). Key NOEs and associated conformers are noted. a-1) Regular 1D spectrum. a-2) Inversion of Man H-1′. For **1**, NOEs at Man H-2′ (intraresidual 2.5 Å) and Gal H-1 (minimum A, *exo-syn*/*exo-syn*) are similar. An extremely weak NOE at Gal H-2 (minimum C, *exo-syn*/*exo-anti*) is observed. For **2**, the NOE at Man H-2′ (intraresidual 2.5 Å) is much stronger than those at Gal H-1 (minimum A, *exo-syn*/*exo-syn*) and Gal H-2 (minimum C, *exo-syn*/*exo-anti*), which are similar between them. a-3) Inversion of Gal H-1. For **1**, the NOE at Man H-1′ (minimum A, *exo-syn*/*exo-syn*) is ten times stronger than that at Man H-2′ (minimum B, non-*exo*/*exo-syn*). For **2**, the NOE at Man H-1′ (minimum A, *exo-syn*/*exo-syn*) is slightly weaker than that at Man H-2′ (minimum B, non-*exo*/*exo-syn*). b) Build-up curves corresponding to the key NOEs H1-H1′ (red) and H1-H2′ (blue). NOE volumes were normalized with respect to the diagonal peak at every mixing time.

  0947-6539/00/0606-1037 $ 17.50+.50/0

full optimizations of the MM3* minima obtained for **1** and **2** were performed at the ab initio level by using the 6-31G* basis set. Simplified models of **1** and **2** were built including only the hydroxyl group at position 2 in both pyranose rings. The C6-hydroxymethyl groups were not considered. ϕ_{Man}/ϕ_{Gal} values of the minimized geometries and the corresponding energies and populations are shown in Table 1. For compound **1**, the ab initio optimization of the MM3* energy minima led to only

Table 1. Torsion angle values, relative energies, and populations according to MM3* and 6–31G* calculations for the different minima of compound **1** and **2**. Those geometries obtained by partial optimization are marked with (*). Energy values are given in kcal mol^{-1}.

	MM3*			6–31G*		
Minima	Φ_{Man}/Φ_{Gal}	ΔE	*Pop* [%]	Φ_{Man}/Φ_{Gal}	ΔE	*Pop* [%]
Compound **1**						
A	– 47.0/63.1	0	> 99	– 52.0/13.7	0	70.9
B	43.0/58.2	3.37	< 1	40.0/44.6	2.61	0.97*
C	– 41.4/165.8	3.39	< 1	– 32.6/171.9	0.66	23.5
D	– 61.8/ – 40.0	3.66	< 1*	– 52.0/ – 40.0	1.64	4.63*
E	40.0/157.1	6.48	< 1*	40.0/ – 165.9	4.91	< 0.1*
Compound **2**						
A	– 47.5/57.0	0	66.8	– 63.6/29.7	0.29	20.9
B	52.6/58.9	0.71	20.4	45.6/56.1	0.15	26.4
C	– 46.0/171.2	1.84	3.3	– 46.6/171.6	0	33.9
D	– 66.3/ – 56.6	1.24	8.4	– 57.0/ – 28.3	0.43	16.4
E	55.0/ – 173.3	2.42	1.1	58.1/ – 168.7	1.58	2.4

two low-energy geometries, since the minimization of those conformers characterized by non-*exo*-anomeric orientations for either ϕ_{Man} or ϕ_{Gal} converged to the closest *exo*-anomeric geometry. Thus, to get an estimation of the ab initio energy differences between the *exo*- and non-*exo* orientations for ϕ_{Man} and ϕ_{Gal}, partial optimizations of the MM3* non-*exo*-anomeric minima were carried out, keeping ϕ_{Man} or ϕ_{Gal} angles fixed at their corresponding non-*exo*-anomeric values. Those conformers characterized by *exo-syn* or *exo-anti* orientations were fully optimized. ϕ_{Man}/ϕ_{Gal} values of the obtained geometries and their corresponding energies and populations are shown in Table 1. All the five minima were obtained for compound **2**.

Some differences with respect to the MM3* values can be observed. For compound **2**, the Hartree-Fock calculations predict very small energy differences between four of the minima. Indeed, although the global minimum is now located in the *exo-syn*/*exo-anti* region characterized by ϕ_{Man}/ϕ_{Gal} 46/171, the 6-31G*-based populations for minima A–D oscillate between 16 and 34%. For compound **1**, as also observed for the MM3* map, the global minimum is located in the *exo-syn*/*exo-syn* region (minimum A). While, the ab initio calculations predict that the presence of non-*exo*-anomeric conformers for **1** is around 5%, for **2** these non-*exo* conformers amount to 45%. Both methods also show the different conformational behavior of **1** and **2** in terms of the cost of torsional changes. According to the HF/6-31G* calculations, for compound **1**, the transition between minimum A (the global minimum) and minimum B (characterized by a non-*exo*-anomeric orientation around ϕ_{Man}) has an energy cost of 2.61 kcal mol^{-1}. In contrast, for **2**, the same conformational change is now favored by – 0.14 kcal mol^{-1} (Figure 5).

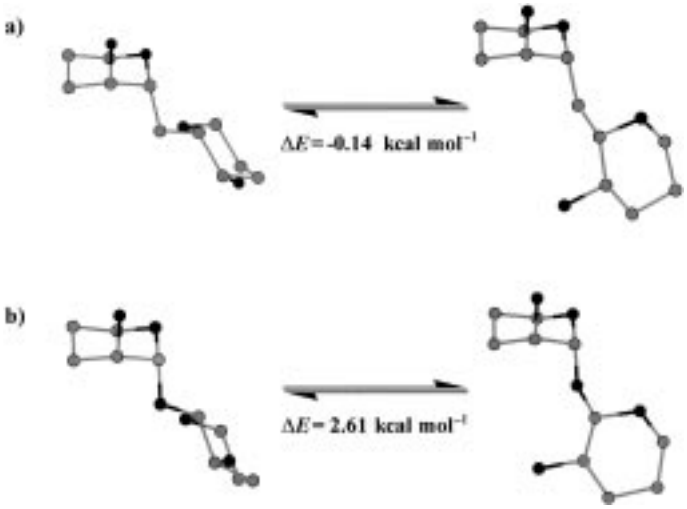

Figure 5. Schematic representation of the conformational change between minimum A and minimum B. The estimation of the energy cost for the transition according to HF 6–31G* calculations in both the O-disaccharide and in the C-analogue is shown.

Molecular dynamics simulations: In a first step, six non-restrained MD simulations were performed using three different values of dielectric constant ($\varepsilon = 1$, $\varepsilon = 1 \times r$, $\varepsilon = 80$) and two starting geometries of compounds **1** and **2** (minima A and B). Explicit solvent molecules and periodic boundary conditions were used in the calculations with $\varepsilon = 1$. Some of the rotamer distributions around ϕ_{Man}/ϕ_{Gal} obtained for **2** are shown in Figure 6. Although the final results of these non-restrained computations are very sensitive to the conditions used in the simulation, all the trajectories agree with an enhanced flexibility of **2** in comparison with **1**, especially for the ϕ_{Man} linkage. The best fit of the experimental data was obtained with $\varepsilon = 1 \times r$ (with maximum differences in *J* values of around 1 Hz and small deviations from the NMR derived average distances).

Then, as a further step, and in order to get the *best experimental* conformer distribution, for both **1** and **2**, time averaged restrained (tar)-MD simulations[11] were carried out using the AMBER 5.0 force field[12] and the experimental NOE/*J* information. NOE-derived distances were included as time averaged distance constraints and scalar coupling constants as time averaged *J* coupling restraints. Three NOEs were used for **1**, while 14 NOE and four *J* values were used for **2**. Four 15 ns trajectories were collected for each molecule: Two different starting geometries (minimum A and minimum B) and two different dielectric constants ($\varepsilon = 1 \times r$ and $\varepsilon = 80$) were used as input. The distributions of rotamers around ϕ_{Man}/ϕ_{Gal} for **2** are shown in Figure 6. In all cases, basically identical outputs were obtained, independent from the starting geometry. In addition, a very small influence of the dielectric constant values on the final results was observed. These results clearly indicates that the simulations lengths are adequate for the proper convergence of the conformational parameters for these systems.[13] Overall, the simulations which used $\varepsilon = 1 \times r$ produced the best fit of the experimental data (*J* and NMR derived distances, see Tables 2 and 3). The new distribution produced for **1** is shown in Figure 7. Minimum A (*exo-syn*/*exo-syn*) is the major one (now 93%), while

0947-6539/00/0606-1038 $ 17.50+.50/0 *Chem. Eur. J.* **2000**, *6*, No. 6

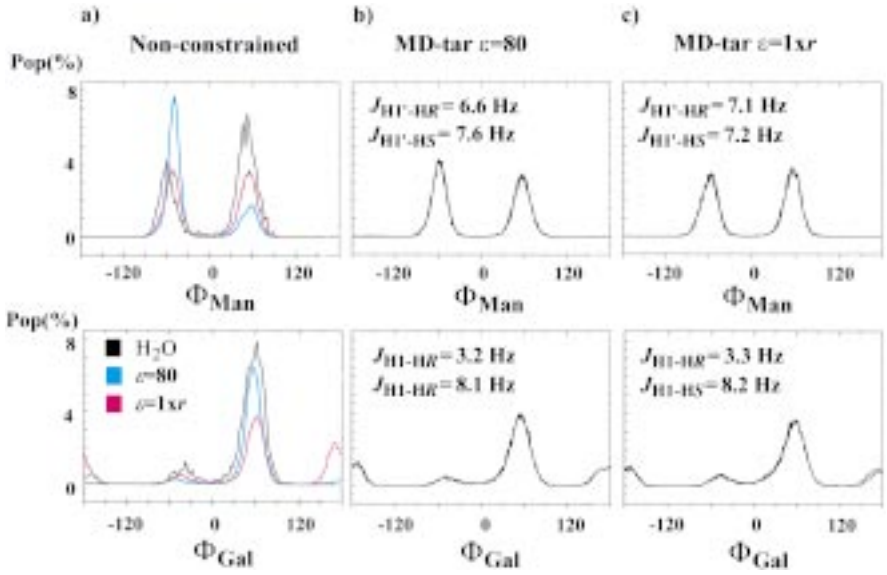

Figure 6. a) Distributions of rotamers around ϕ_{Man} and ϕ_{Gal} obtained from three independent non-restrained MD simulations, using explicit solvent and periodic boundary conditions (black), $\varepsilon = 80$ (blue) and $\varepsilon = 1 \times r$ (red). b) Distributions of rotamers around ϕ_{Man} and ϕ_{Gal} obtained from two independent MD-tar simulations using minima A and B as starting geometries and $\varepsilon = 80$. The predicted J values are shown. c) Distributions of rotamers around ϕ_{Man} and ϕ_{Gal} obtained from two independent MD-tar simulations using minima A and B as starting geometries and $\varepsilon = 1 \times r$. The predicted J values are shown.

Table 2. Experimental values for the vicinal proton–proton coupling constants [Hz] for the pseudoglycosidic linkage. The values calculated (using the complete Karplus–Altona equation) through tar- and non-restrained (in vacuo and solvated) molecular dynamics simulations are also given, along with the corresponding starting geometry. The best fit is given in bold.

	J(H1′,H_R)	J(H1′,H_S)	J(H1,H_R)	J(H1,H_S)
Exp	7.1	7.4	3.1	8.0
MD-tar/$\varepsilon = r$ Min A	6.9	7.3	3.5	8.0
MD-tar/$\varepsilon = r$ Min B	7.1	7.2	3.4	8.2
MD-tar/$\varepsilon = 80$ Min A	6.6	7.6	3.2	8.1
MD-tar/$\varepsilon = 80$ Min B	6.5	7.6	3.3	8.0
$\varepsilon = 80$ Min A	3.8	9.1	2.6	10.1
$\varepsilon =$ r Min A	6.6	7.0	3.9	7.3
H_2O Min A	8.0	5.9	3.0	9.9

B (non-*exo*/*exo-syn*) is populated about 4% and C 2%. However, with only three NOEs being consider, it is still possible that distributions of other conformations could fit the NOE data.[10] The obtained result is in perfect agreement with the MM3* predictions. In contrast, the single-point ab initio calculations are only qualitatively in agreement with the MD-tar distribution, since they clearly overestimate the population around minimum C. A population of 23% around this mimimum would produce a H1′-H2 NOE much stronger than the observed one. Nevertheless, since we have deduced single point values and the HF/6-31G* calculations have been performed in vacuo, this result can be considered satisfactory.

The distribution obtained for **2** is shown in Figure 7. Now, the *observed* J(4)/NOE(14) data with conformational information are in full concordance with the values *calculated* from the MD (Tables 2 and 3), and demonstrate the different conformational behavior of C-glycoside **2** compared with **1**. Indeed, the Φ_{Man} orientations are quite different. Φ_{Man} of **2** is very flexible. There is a 52% population of conformers with Φ_{Man} 60° (i.e., not favored by the *exo*-anomeric effect) compared with only 4% for **1**. By comparison, the conformational distribution about the β–Φ_{Gal} linkage is more similar. There is an increase of 12% population of non-*exo* conformers, while their presence in **1** in less than 1%. Presumably, the equatorial orientation of Gal O-2 destabilizes the non-*exo* conformers through 1,3-like diaxial interactions, thereby reducing the differences between **1** and **2**. Therefore, the β-Φ_{Gal} linkage of **2** is more rigid than the α-

Table 3. Experimental and calculated inter-residue proton–proton distances with conformational information for **1** and **2** for the best tar-MD simulations. The starting geometry and dielectric conditions are also given.

H/H pair	exp	tar-MD/Min A $\varepsilon = 80$	tar-MD/Min B $\varepsilon = 80$
Compound 1			
H1′/H1	2.20–2.50	2.36	2.36
H1′/H2	3.60–4.00	4.08	4.16
H2′/H1	3.50–3.90	3.51	3.48
H2′/H2	>4.20	4.58	4.60
H/H pair	exp	tar-MD/Min B $\varepsilon = r$	tar-MD/Min B $\varepsilon = 80$
Compound 2			
H1′/H1	2.60–2.90	2.79	2.76
H1′/H2	3.00–3.40	3.10	3.09
H2′/H1	2.50–2.80	2.56	2.59
H2′/H2	>3.30	3.49	3.43
H_R/H2′	2.40–2.70	2.62	2.58
H_R/H3′	2.40–2.70	2.53	2.56
H_R/H5′	2.40–2.70	2.48	2.50
H_R/H2	2.70–3.00	2.83	2.89
H_S/H3′	2.50–2.80	2.59	2.54
H_S/H5′	2.30–2.60	2.49	2.46
H_S/H2	2.55–2.85	2.63	2.66

Φ_{Man} analogue (see [7b] for a completely different conclusion). These results also indicate that C-glycosides may display significant variations, not only around Ψ as C-lactose,[5] but also around Φ.

The importance of stereoelectronic effects in determining the preferred conformation of O-glycosides has been questioned.[7] The *experimental* difference in conformational mobility in **1** and **2** suggests otherwise. Assuming that the magnitudes of the inter-residue interactions are not significantly affected by the difference in C–O versus C–C bond distances in the linker, the A/B conformer distributions in **1** and **2** would be expected to be similar in the absence of a

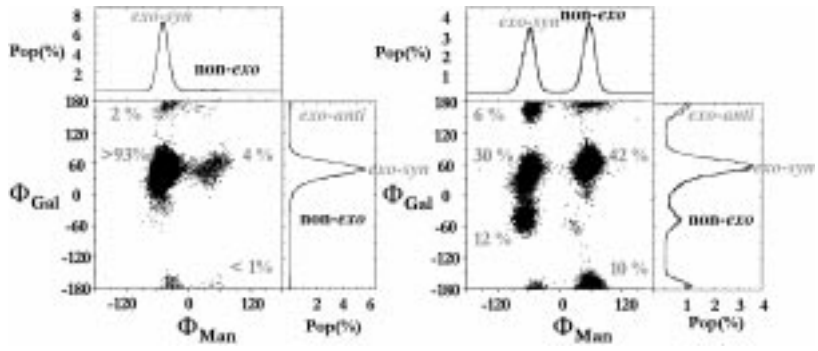

Figure 7. Trajectories of two independent 15 ns tar-MD simulations ($\varepsilon = 1 \times r$) performed for **1** (left) and **2** (right) with AMBER 5.0. Four MD simulations were performed in total for each compound. Three NOEs were included for **1** and 14 NOEs and four coupling constants were included for **2**. The agreement between the back calculated NMR parameters and the observed ones was excellent. The populations of every conformational family are given. The top and right traces show the percentage of populations at any orientation (*exo-syn*, non-*exo*, *exo-anti*). The results of two of the simulations are superimposed. The difference between Φ_{Man} of **1** and **2** is evident. There are also differences for Φ_{Gal}.

stereoelectronic effect. That conformer A is strongly preferred in **1** (compared with a preference for B in **2**) is consistent with the importance of the stereoelectronic effect. The absence of a C2-equatorial substituent in the mannose residue, the existence of a 1,3-type diaxial interaction between the C1′–O5′ and C1–O5 bonds in conformer A, and the shorter C–O bond distance in **1** would if anything suggest a *higher* B/A ratio for **1** compared with **2**, in contrast to the experimental observation. Therefore, the comparison of the B/A ratios for **1** and **2** should give a lower limit for the stereoelectronic effect in water (for Φ_{Man} of **1**, 2.1 kcal mol^{-1} corresponding to A:B from 96:4 to 30:42). Since the *exo*-anomeric effects for trehalose-like systems are opposed, this value is expected to be smaller than the *exo*-anomeric effect for regular saccharides.[6c]

Conclusion

In summary, the greater flexibility around the C-glyconic bond in **2** compared with **1** is strongly indicative of a stereoelectronic basis for the *exo*-anomeric effect. This factor must be therefore considered when comparing conformations of O- and C-glycosides. Our finding that the axial-glyconic bond is less rigid than the equatorial one is in contrast with previous reports on similar α,β-(1→1) systems.[7b] The implication of C-glycoside flexibility is that conformers other than the ground state may be bound in the binding site of proteins without major energy conflicts. When a lectin imposes a constraint by establishing interactions to both sugar units, then only a certain topologically favored conformer will fit into the binding site. Increased binding affinity may result if the enthalpic gains exceed the entropic penalty.[5a,b] Therefore, C-glycosides are excellent probes to study[5, 7] the binding of proteins or enzymes and are important for drug design.[5a–c]

Experimental Section

Materials: The synthesis of **1** and **2** has been described elsewhere.[14]

Calculations: Potential energy surfaces were calculated with the MM3* force field as included in Macromodel 4.5.[15] A dielectric constant of 80 was used.

For the tar-MD simulations, compounds **1** and **2** were built using the X-Leap[16] program. Atomic charges were derived from AM1 semiempirical calculations. All molecular dynamics simulations were carried out using the Sander module within the AMBER 5.0 package. As a first step, six non-restrained MD simulations were run for both compounds, three starting from minimum A (*exo-syn*/*exo-syn*) and three starting from minimum B (non-*exo*/*exo-syn*). Two 500 ps trajectories were recorded using $\varepsilon = 1$ and explicit solvent. A single molecule of **1** or **2** was immersed into a box with 758 TIP3P water molecules. Periodic boundary conditions were used. As a first step, a short constant pressure equilibration was performed until a final density of 1 g cm^{-3} was obtained. A cutoff of 10 Å was used for non-bonding interactions. Four 15 ns simulations were run using $\varepsilon = 1 \times r$ and $\varepsilon = 80$ with no explicit solvent.

In addition, MD-tar simulations were carried out for **1** and **2**. NOE-derived distances were included as time averaged distance constraints and scalar coupling constants as time averaged J coupling restraints. A $\langle r^{-6}\rangle^{-1/6}$ average was used for the distances and a linear average was used for the coupling constants. The J values are related to the torsion τ by the well known Karplus relationship:[17]

$$J = A\cos^2(\tau) + B\cos(\tau) + C$$

A, B, and C values were chosen to fit the extended Karplus–Altona relationship[18] for every particular torsion. At the end of the simulations the averaged J values were calculated using both the regular Karplus and the complete Altona equations and compared with the experimental ones.

Trial simulations were run using different simulation lengths (between 1 and 15 ns) and different force constants for the distances (between 10 and 30 kcal mol^{-1} Å^{-2}) and J couplings (between 0.1 and 0.3 kcal mol^{-} Hz^{-2}) constraints. Different values for the exponential decay constant(between 100 ps and 1.5 ns) were also tested. These preliminary runs showed that for flexible molecules such as **1**, the use of exponential decay constants shorter than 1 ns produced unstable trajectories and led in some cases to severe distortions of the pyranose rings. In contrast, good results were obtained when using exponential decay constant values of 1 ns or larger. It has been estimated[19] that simulation lengths of about one order of magnitude larger than the exponential decay constant should be used to generate reliable estimates of average properties. Thus, the final trajectories were run using an exponential decay constant of 1.5 ns and a simulation length of 15 ns.

It is also known[11] that when using large force constants for the J coupling constraints, the molecule can get trapped in high energy, physically improbable, incorrect minima. In order to solve this false minima problem, low values (between 0.1 and 0.3 kcal mol^{-} Hz^{-2}) were used for the J coupling restraints force constants.

Four final 15 ns MD-tar simulations (two starting from minimum A and two starting from minimum B) were run for each molecule (**1** and **2**) using two different dielectric constant values ($\varepsilon = 80$ and $\varepsilon = 1 \times r$). Population distributions obtained starting from different initial geometries were almost identical indicating that the simulation length is adequate for a proper convergence of the conformational parameters. In addition, very similar results were obtained for both dielectric constant values indicating a rather small influence of the force field in the final results. Average distance and J values obtained in this way were found to correctly reproduce the experimental values.

ab initio Calculations were performed with the Gaussian 98 program.[20] Simplified models of **1** and **2** were built including only the hydroxyl group at position 2 for both pyranose rings. MM3* minima were optimized by HF calculations with the 6-31G* basis set. In the case of **1**, for those conformers characterized by non-*exo*-anomeric orientations of ϕ_{Man} (minima B and E) this angle was kept fixed ($\phi_{Man} = 40°$) during the minimization process. In a similar way, those conformers characterized by non-*exo*-anomeric orienta-

0947-6539/00/0606-1040 $ 17.50+.50/0 *Chem. Eur. J.* **2000**, *6*, No. 6

tions of ϕ_{Gal} (minimum D) were minimized keeping this angle fixed ($\phi_{Gal} = -40°$).

NMR spectroscopy: The NMR experiments were recorded on a Varian Unity 500 spectrometer. 2D NOESY experiments used the standard sequence, while 1D selective NOE spectra were acquired using the double echo sequence proposed by Shaka and co-workers.[21] Five different mixing times were used for the 1D NOE experiments: 200, 400, 600, 800, and 1000 ms. Cross relaxation rates were estimated from these measurements and the determination of proton–proton distance restrictions was carried out from several known intraresidue distances according to a full relaxation matrix analysis with 80 ps correlation time.

Acknowledgment

Financial support by DGICYT (Spain, Grant PB96-0833) is acknowledged. J.L.A. thanks CAM and MEC for a fellowship. This work was also supported by grants from the US National Institutes of Health (RR0307 and GM-57865).

[1] H. J. Gabius, S. Gabius (eds.), *Glycosciences: Status and Perspectives*, Chapman&Hall, London, **1997**.
[2] M. L. Philips, E. Nudelman, F. C. A. Gaeta, M. Perez, K. Singhal, S. Hakomori, J. C. Paulson, *Science* **1990**, *250*, 1132.
[3] W. Levy, D. Chang (Eds.), *Chemistry of C-glycosides*, Elsevier, Cambridge, **1995**.
[4] R. Weatherman, L. Kiessling, *J. Org. Chem*. **1996**, *61*, 534–538.
[5] a) J. F. Espinosa, F. J. Cañada, J. L. Asensio, M. Martín-Pastor, H. Dietrich, M. Martín-Lomas, R. R. Schmidt, J. Jiménez-Barbero, *J. Am. Chem. Soc.* **1996**, *118*, 10862–10871; b) J. F. Espinosa, J. Cañada, J. L. Asensio, H. Dietrich, M. Martín-Lomas, R. R. Schmidt, J. Jiménez-Barbero, *Angew. Chem.* **1996**, *108*, 323–326; *Angew. Chem. Int. Ed. Engl.* **1996**, *35*, 303–306; c) J. F. Espinosa, E. Montero, A. Vian, J. Garcia, H. Dietrich, M. Martín-Lomas, R. R. Schmidt, A. Imberty, J. Cañada, J. Jiménez-Barbero, *J. Am. Chem. Soc.* **1998**, *120*, 10862–10871; d) J. F. Espinosa, M. Bruix, O. Jarreton, T. Skrydstrup, J.-M. Beau, J. Jiménez-Barbero *Chem. Eur. J.* **1999**, *5*, 442–448.
[6] a) R. U. Lemieux, S. Koto, D. Voisin, *ACS Symp. Ser*. **1979**, *87*, 17–29; b) For ab initio calculations on O-C-C-C systems, see K. N. Houk, J. E. Eksterowicz, Y.-D. Wu. C. D. Fuglesang, D. R. Mitchell, *J. Am. Chem. Soc.* **1993**, *115*, 4170–4177; c) A value of 1.9 kcal mol^{-1} has been calculated for axial 2-O-methyl oxane, see I. Tvaroska, T. Bleha, *Adv. Carbohydr. Chem. Biochem.* **1989**, *47*, 45–103.
[7] a) R. Ravishankar, A. Surolia, M. Vijayan, S. Lim, Y. Kishi, *J. Am. Chem. Soc.* **1998**, *120*, 11297–11303, and references therein; b) A. Wei, Y. Kishi, *J. Org. Chem.* **1994**, *118*, 88–96, and references therein.
[8] K. Hiruma, T. Kajimoto, G. Weitz-Schmidt, I. Ollman, C.-H. Wong, *J. Am. Chem. Soc.* **1996**, *118*, 9265–9270.
[9] J. Dabrowski, T. Kozar, H. Grosskurth, N. E. Nifant'ev, *J. Am. Chem. Soc.* **1995**, *117*, 5534.
[10] D. Neuhaus, M. P. Williamson, *The NOE in structural and conformational analysis*, VCH, New York, **1989**.
[11] D. A. Pearlman, *J. Biomol. NMR* **1994**, *4*, 1–16; D. A. Pearlman, *J. Biomol. NMR* **1994**, *4*, 279–299.
[12] D. A. Pearlman, D. A. Case, J. W. Caldwell, W. S. Ross, T. E. Cheatham III, S. DeBolt, D. Ferguson, G. Siebal, P. Kollman, *Comp. Phys. Commun*. **1995**, *91*, 1–41.
[13] D. A. Pearlman, P. A. Kollman, *J. Mol. Biol*. **1991**, *220*, 457–479.
[14] N. Khan, X. Chen, D. R. Mootoo, *J. Am. Chem. Soc*. **1999**, *121*, 4918–4919.
[15] F. Mohamadi, N. G. J. Richards, W. C. Guida, R. Liskamp, C. Caufield, G. Chang, T. Hendrickson, W. C. Still, *J. Comput. Chem.* **1990**, *11*, 440–467.
[16] C. E. A. F. Schafmeister, W. S. Ross, V. Romanovski, *LEaP*, University of California, San Francisco, **1995**.
[17] M. Karplus, *J. Chem. Phys.* **1959**, *30*, 11.
[18] C. A. G. Haasnoot, F. A. A. M. de Leeuw, C. Altona, *Tetrahedron* **1980**, *36*, 2783–2792.
[19] A. E. Torda, R. M. Scheek, W. F. van Gunsteren, *Chem. Phys. Lett.* **1989**, *157*, 289–294.
[20] M. J. Frisch, G. W. Trucks, H. B. Schlegel, G. E. Scuseria, M. A. Robb, J. R. Cheeseman, V. G. Zakrzewski, J. A. Montgomery Jr., R. E. Stratmann, J. C. Burant, S. Dapprich, J. M. Millam, A. D. Daniels, K. N. Kudin, M. C. Strain, O. Farkas, J. Tomasi, V. Barone, M. Cossi, R. Cammi, B. Mennucci, C. Pomelli, C. Adamo, S. Clifford, J. Ochterski, G. A. Petersson, P. Y. Ayala, Q. Cui, K. Morokuma, D. K. Malick, A. D. Rabuck, K. Raghavachari, J. B. Foresman, J. Cioslowski, J. V. Ortiz, B. B. Stefanov, G. Liu, A. Liashenko, P. Piskorz, I. Komaromi, R. Gomperts, R. L. Martin, D. J. Fox, T. Keith, M. A. Al-Laham, C. Y. Peng, A. Nanayakkara, C. Gonzalez, M. Challacombe, P. M. W. Gill, B. Johnson, W. Chen, M. W. Wong, J. L. Andres, C. Gonzalez, M. Head-Gordon, E. S. Replogle, and J. A. Pople, *Gaussian*, Inc., Pittsburgh PA, **1998**.
[21] K. Stott, J. Stonehouse, J. Keeler, T. L. Hwang, A. J. Shaka, *J. Am. Chem. Soc.* **1995**, *117*, 4199.

Received: August 10, 1999 [F1967]